

In presenting the dissertation as a partial fulfillment of the requirements for an advanced degree from the Georgia Institute of Technology, I agree that the Library of the Institution shall make it available for inspection and circulation in accordance with its regulations governing materials of this type. I agree that permission to copy from, or to publish from, this dissertation may be granted by the professor under whose direction it was written, or, in his absence, by the dean of the Graduate Division when such copying or publication is solely for scholarly purposes and does not involve potential financial gain. It is understood that any copying from, or publication of, this dissertation which involves potential financial gain will not be allowed without written permission.

^ ^ ^ ^ ^
-v -v -v -v -v

AN INVESTIGATION OF THE DECAY OF ISOTROPIC
TURBULENCE BEHIND A SQUARE MESH GRID
IN A WATER TUNNEL

A THESES

Presented to

The Faculty of the Graduate Division

by

James Rembert DuBose III



In Partial Fulfillment
of the Requirements for the Degree
Master of Science in Civil Engineering


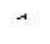

Georgia Institute of Technology

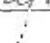
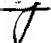
June, 1964

AN INVESTIGATION OF THE DECAY OF ISOTROPIC
TURBULENCE BEHIND A SQUARE MESH GRID
IN A WATER TUNNEL

Approved:

Date approved by Chairman: 5/20/64

ACKNOWLEDGMENTS

I wish to thank those people who have contributed to the success of this work. In particular, I would like to express my sincere appreciation to my theses advisor, Dr. P. G. Mayer, for his guidance and encouragement during this investigation and to Dr. G. M. Slaughter, and Dr. C. W. Gorton for their reading and evaluation of the text.

I also would like to express my appreciation to the United States Geological Survey for its financial assistance and to give special thanks to my wife for her patience, help and understanding.

TABLE OF CONTENTS

	Page
ACKNOWLEDGEMENTS	ii
LIST OF TABLES	v
LIST OF FIGURES	vi
LIST OF SYMBOLS	vii
SUMMARY	x
Chapter	
I. INTRODUCTION	1
II. REVIEW OF THE LITERATURE - PART I	2
Characteristics of Fluid Turbulence	2
Isotropic Turbulence	7
III. REVIEW OF THE LITERATURE - PART II	12
Measurement of Turbulence	12
Hot-Wire Anemometer	13
Constant-Current Anemometer	14
Constant-Temperature Anemometer	16
Glow Discharge Anemometer	18
Hot-Film Anemometer	19
Electromagnetic Induction	20
Total Head Tube with Ceramic Pressure Transducer	22
Electric Spark	25
Shadowgraph	26
Ultramicroscope	28
IV. EXPERIMENTAL APPARATUS	31
Contraction Cone	32
Test Tunnel	32
Pitot-Static Tube	33
Turbulence Probe	34
V. EXPERIMENTAL PROCEDURE	36
Baffling	36

Chapter	Page
Mean Velocity Calibrations	36
Profile Velocity Calibrations	37
Turbulence Behind a Grid	37
VI. DISCUSSION OF RESULTS	38
Tunnel Calibrations	38
Velocity Profiles	38
Turbulence Behind a Grid	39
VII. CONCLUSIONS	41
VIII. RECOMMENDATIONS	42
APPENDIX	43
BIBLIOGRAPHY	57

LIST OF TABLES

Table	Page
1. Cone Coordinates	44
2. Boundary Layer Growth	45
3. Turbulence Intensities	46

LIST OF FIGURES

Figure	Page
1. Grid Forming Isotropic Turbulence	47
2. Side View of Water Tunnel	48
3. Photograph of Water Tunnel.	49
4. Photograph of Contraction Cone	50
5. Velocity-Discharge Relationships	51
6. Velocity Profiles at $R_p = 0.616 \times 10^5$	52
7. Velocity Profiles at $R_p = 1.07 \times 10^5$	53
8. Velocity Profiles at $R_p = 1.68 \times 10^5$	54
9. Turbulence Intensity	55
10. Decay of Grid Turbulence	56

LIST OF SYMBOLS

$\bar{u}, \bar{v}, \bar{w}$	temporal mean velocity component in x, y, and z directions, respectively
u, v, w	instantaneous velocity deviations
t	time
ρ	density
\bar{p}	mean pressure
γ	specific weight
μ	viscosity
$\overline{u^2}, \overline{v^2}, \overline{w^2}$	mean-square values of u, v, w
τ	mean shear stress
η	eddy viscosity
l	mean eddy size; mixing length
u', v', w'	root-mean-square (RMS) values of u, v, w
ϵ	kinematic eddy viscosity
ν	kinematic viscosity
R	correlation coefficient
λ	mean size of the smaller eddies involved in the dissipation process
n	frequency
$F(n)$	mean energy spectrum
\bar{W}	mean rate of energy dissipation
r	radius of pipe
δ	thickness of the boundary layer

d	diameter of wire in grid
M	spacing of grid bars
A_1	constant determined by experiment
x	distance downstream from grid
I	electric current
A_2, B	coefficients of hot-wire characteristics
R_w	electrical resistance of hot-wire
R_g	electrical resistance of a hot wire at gas temperature
U	Eulerian velocity, $\bar{u} + u$
\bar{R}_w	time-mean value
r_w	electrical resistance of the turbulent fluctuation
e	voltage across the hot-wire
s	sensitivity of the hot-wire
H	strength of an electromagnetic field
V	strength of the induced electric field
a	magnetic permeability
c	velocity of light
H_{tg}	instantaneous response of a total head tube
p'	instantaneous pressure
g	acceleration of gravity
$E(n)$	spectral distribution function of longitudinal turbulence
	kinetic energy density per unit mass
u_1, v_1, w_1	maximum values of u, v, w
θ_{xy}, θ_{xz}	maximum values of the angular deviations of flow
m	mean hydraulic depth
D	diameter of pipe

R_m mesh Reynolds number $\bar{u}M/\nu$

R_p pipe Reynolds number $\bar{u}D/\nu$

SUMMARY

Measurement of turbulence components of velocities in water has long been a problem. This study is an attempt to correlate results of turbulence components of velocities measured by the United States Geological Survey with similar measurements made in wind tunnels. An investigation is also made of the velocity profiles and the boundary layer growth.

The first part of this paper gives a description of the water tunnel, contraction cones, and turbulence probe. A discussion of instrumentation and experimental techniques is then given. Measurements of isotropic turbulence behind a 1/2 inch grid were obtained and compared with wind tunnel data.

The results indicated that the center portion of the tunnel was free of velocity gradients, and hence, apparently free from viscous shear and could theoretically have isotropic turbulence. The results showing decay of isotropic turbulence are presented.

It was concluded that the magnitude of u'/\bar{u} versus R_m was in the right order of magnitude, but that the decay of isotropic turbulence was less than expected when compared to wind tunnel tests.

CHAPTER I

INTRODUCTION

The purpose of this investigation was to study the feasibility of a water tunnel as a tool for calibrating turbulence probes at the Georgia Tech Hydraulics Laboratory. Turbulence measuring devices can only be calibrated in known turbulence fields. Isotropic turbulence is a known type of turbulence with definite and predictable characteristics.

Decay of isotropic turbulence in wind tunnels has been conducted many times. However, an investigation of the decay of isotropic turbulence in a water tunnel has not been performed satisfactorily to date. Attempts have been made to measure turbulence in water by means of hot film anemometers, total head tubes, etc., but all have failed to give consistently satisfactory results.

The investigation was performed in a water tunnel designed and built in the Georgia Tech Hydraulics Laboratory, using a total-head type probe developed by the United States Geological Survey.

CHAPTER II

REVIEW OF THE LITERATURE - PART I

Characteristics of Fluid Turbulence

Fluid turbulence is a phenomenon in which eddies generated in an initial zone of instability spread rapidly over the entire flow section, thereby producing a complex pattern of motion which varies continuously with time. The complex secondary motion superimposed upon the primary motion of translation is the major distinction between turbulent and laminar flow. After the flow is established and everywhere rotational, the influence of wall friction is felt throughout the flowfield (1)*. When this happens the rate of energy dissipation is greatly increased. If a sensitive velocity meter is immersed in the turbulent stream, continual deviations from the mean would result due to these eddies which move in every direction. There will be a statistical lower limit to the size of the smallest eddy due to greater velocity gradients of the smaller eddies and greater viscous shear stress (2).

Osbrone Reynolds, in order to simplify the continuity equation and the Navier-Stokes equation, substituted for every instantaneous velocity component the sum of the temporal mean exponent \bar{u} and the instantaneous component u . Introduction of these identities and elimination of all terms having a mean value of zero, resulted in

*Numbers in parentheses refer to items in the Bibliography.

the continuity equation

$$\frac{\partial \bar{u}}{\partial x} + \frac{\partial \bar{v}}{\partial y} + \frac{\partial \bar{w}}{\partial z} = 0$$

and three equations of the form,

$$\begin{aligned} \frac{\partial \bar{u}}{\partial t} + \bar{u} \frac{\partial \bar{u}}{\partial x} + \bar{v} \frac{\partial \bar{u}}{\partial y} + \bar{w} \frac{\partial \bar{u}}{\partial z} = - \frac{1}{\rho} \frac{\partial}{\partial x} (\bar{p} + \gamma z) \\ + \frac{\mu}{\rho} \left(\frac{\partial^2 \bar{u}}{\partial x^2} + \frac{\partial^2 \bar{u}}{\partial y^2} + \frac{\partial^2 \bar{u}}{\partial z^2} \right) - \frac{\partial \bar{u}^2}{\partial x} - \frac{\partial \bar{uv}}{\partial y} - \frac{\partial \bar{uw}}{\partial z} \end{aligned} \quad (3)$$

The effect of the turbulence is embodied in the three mean products of the components of fluctuation.

The basic significance of the Reynolds equation in steady, uniform turbulence flow results when they are reduced to

$$\bar{\tau} = \mu \frac{d\bar{u}}{dy} - \rho \bar{uv}$$

The contribution of the turbulent motion to the local shear depends upon the magnitude of the mean product \bar{uv} . Only if there is an appreciable correlation of the two components can the mean product have a definite magnitude. In isotropic turbulent flow behind a screen or grid, these Reynolds stresses are zero, showing complete lack of correlation and hence, zero shear.

If the analogy between microscopic molecular motion and macroscopic eddy motion of fluid turbulence is made, it will be seen that the eddy viscosity η should depend upon the density of the fluid, the mean

eddy size l of the eddies, and the root-mean-square u' of the instantaneous velocity deviation from the mean velocity. Accordingly, Boussinesq reasoned that

$$\bar{\tau} = (\mu + \eta) \frac{d\bar{u}}{dy} \quad (4)$$

The parameter η is a characteristic of fluid motion whereas μ is a fluid property. If η is divided by ρ there is obtained a factor which is characteristic of the flow alone,

$$\eta/\rho = - \frac{\overline{uv}}{d\bar{u}/dy} = \epsilon$$

The factor ϵ is a kinematic eddy viscosity comparable to ν , the kinematic molecular viscosity.

The actual interrelationship of the Reynolds and the Boussinesq parameters is clarified by Prandtl's mixing length theory. Prandtl proposed that small aggregations of fluid particles are transported by turbulence a certain mean distance l (mixing length), from regions of one velocity to regions of another and in so doing, suffer changes in their general velocities of motion. Prandtl suggested that the change in velocity $d\bar{u}/dy$ incurred by a fluid particle moving through the distance l was proportional to u' and v' . That is

$$u' \propto v' \propto l \frac{d\bar{u}}{dy}$$

The idea underlying Prandtl's hypothesis is Fage and Townend's observations that the three components of turbulent velocity tend to be equal

to one another in the center of the pipe (6). If the assumption is made that the mean product of the components may be replaced by the respective terms of the foregoing proportionalities, it will follow that

$$\epsilon = 1 u'$$

From statistical processes in a circular pipe, it has been shown that the proceeding product is a maximum approximately midway between the wall of the pipe and the centerline. The product is frequently called the diffusion coefficient and is important in analysis of energy dissipation, problems of heat transfer, and the suspension of finely divided material by the process of turbulent convection.

The velocity characteristic can be determined from statistical analysis of the RMS values of the instantaneous velocity fluctuations. The length scale involves the measurement of the correlation between two neighboring velocity indicators as the distance between them is varied. The indicators would show perfect correlation when they are superimposed. The correlation would approach zero as the indicators are moved apart until their spacing exceeded the mean eddy size. The correlation coefficient is given by

$$R = \frac{\overline{(u)_1 (u)_2}}{\overline{(u)_1^2}}$$

A plot of the correlation coefficient (ordinate) against spacing of the indicators (abscissa) will yield a curve, the area of which is equal to 1 (mean eddy size). If a parabola is fitted to the peak of the correlation

curve and allowed to intercept the abscissa, there is a value λ obtained which is defined as the mean size of the smaller eddies involved in the process of dissipation of energy. With the RMS value and the mean eddy size determined by statistical method, the diffusion coefficient can be determined.

Eddies of various sizes of which turbulent motion is composed, have a certain kinetic energy determined by the intensity of the velocity fluctuation of the corresponding frequency. Although in real turbulence a distinct frequency is not permanently present, it is possible on the average to allocate a certain amount of the total energy to a distinct frequency. A distribution of the energy between the frequencies is called an energy spectrum. The largest eddies will cause fluctuations of low frequencies and the smallest eddies will cause fluctuations of high frequencies. There is a minimum scale of turbulence that corresponds to a maximum frequency in the turbulent motion. One may anticipate that when the correlation curve has a small spread in the abscissa co-ordinate, the spectrum curve will extend to large values of n (frequency) and vice versa. The spectrum curve and the correlation curve are Fourier transforms of one another. G. I. Taylor (7) found these related equations to be:

$$R = \int_0^{\infty} F(n) \cos \frac{2\pi nx}{\bar{u}} dn$$

and

$$F(n) = \frac{4}{\bar{u}} \int_0^{\infty} R \cos \frac{2\pi nx}{\bar{u}} dx$$

where $F(n)$ is the mean energy spectrum. It should be pointed out that the area covered by the energy spectrum curve should be equal in unity. That is,

$$\int_0^\infty F(n) \, dn = 1$$

Isotropic Turbulence

Isotropic turbulence may be defined by the condition that the average value of any function of the velocity components and their space derivatives at a particular point, defined in relation to a particular set of axes, is unaltered by any rotation or reflection of the axes of reference (8).

Isotropic turbulence is studied extensively because a knowledge of its characteristics may still form a fundamental basis for the study of actual, nonisotropic turbulent flows. Isotropic turbulence is more amenable to theoretical treatment and theoretical relations may be checked more easily by suitable experiments than any other type of turbulence. In wind tunnel technique it is of great importance to be able to estimate the degree of turbulence on the application of tunnel results to the problems confronting the designer.

Screens or grids may be used to augment the turbulence in a wind tunnel. Isotropic turbulence in a water tunnel can only exist so long as the boundary layer, which is a region near the surface of the wall of the tunnel where the velocity changes from that of the body right at the surface to the velocity of the free stream some distance away, does not interfere with the central portion of the tunnel (9). In conduit flow, the thickness of this boundary layer increases downstream until

it becomes equal to the radius of the conduit. Until this happens the frictional aspects of the flow are confined to the boundary layer where the flow is rotational. Outside the boundary layer the viscosity of the fluid is inoperative and the flow here is frictionless or irrotational and the Reynolds' stresses are zero. In this cone of fluid the total head may be considered constant. Since the flux across any section is constant, and since the boundary layer thickness is increasing, this cone is accelerated, accompanied by a corresponding fall in pressure (10).

Isotropic turbulence can be produced in a tunnel by means of a grid of wire mesh placed at the upstream end. Such grids are used when turbulence effects are being studied, since they are the only convenient way of producing varying degrees of turbulence in the same tunnel. This grid causes eddies to be shed equally in all directions, a condition necessary for isotropic turbulence. See Figure 1 for an illustration. Turbulent motion is here considered to be a mixture of eddies of all sizes from the largest, where dimensions are comparable to the grid of bars in the tunnel, down to the smallest eddies. When turbulent motion starts, the eddies produced by the grid break up the flow into smaller eddies and so on. The grid will set up at first an eddy motion of a nonuniform and nonisotropic character. Further downstream where the individual wakes of the bars (called "shadow" of the grid by G. I. Taylor) has disappeared and the imposed pattern has been wiped out, the mean velocity becomes uniform and there is a strong tendency toward isotropy (11).

As reported by C. Cometta (12), an anomalous behavior of the flow characteristics was observed when wall effects interfered. In the design of an experimental apparatus, the turbulence created at the side walls

and diffused into the main stream must be kept to a minimum.

The rate at which the energy of isotropic turbulence is dissipated is directly proportional to the velocity of fluctuation and inversely proportional to the scale of the eddies. The general expression for the mean rate of dissipation is

$$\bar{W} = 15\mu \left(-\frac{u'}{\lambda}\right)^2$$

Since u' and λ can be measured by turbulence instruments, the relationship can be verified if \bar{W} can be measured by another method. The mean rate of loss of kinetic energy per unit volume in isotropic turbulence is $-3/2 \rho \bar{u} d(u')^2/dx$. This must be equal to \bar{W} so that

$$-\frac{3}{2} \rho \bar{u} \frac{d(u')^2}{dx} = 15\mu \left(-\frac{u'}{\lambda}\right)^2$$

and all the quantities in this equation can be measured.

In a pipe the dissipation of energy is proportional to $\rho (u')^3 r^{-1}$, where r is the radius of the pipe. It was supposed that the dissipation of turbulence \bar{W} behind geometrically similar grids is proportional to $(u')^3 L^{-1}$ where L is any linear dimension which defines the scale of the turbulence producing mechanism. The mesh length M was taken as the typical length L . Therefore,

$$\frac{\lambda}{M} = A_1 \sqrt{\frac{\nu}{Mu'}}$$

where A_1 is a constant to be determined by experiment.

With the expression

$$\frac{\lambda}{M} = A_1 \sqrt{\frac{\nu}{Mu'}}$$

G. I. Taylor (13) integrated the equation

$$-\frac{3}{2} \rho \bar{u} \frac{d(u')^2}{dx} = 15\mu \left(\frac{u'}{\lambda}\right)^2$$

for λ to give

$$\frac{\bar{u}}{u'} = \frac{5x}{A_1^2 M} + \text{constant}$$

where A_1 is a constant ranging from 1.95 to 2.20 by experiment.

There are certain limitations to this law which are:

- (1) It cannot be applied when $Mu' \sqrt{\nu}$ is small.
- (2) It does not apply immediately behind the grid where the "shadow" of the grid is still distinct.
- (3) The law does not apply where the existing turbulence is not entirely due to the grid.

This theoretical law for the decay of turbulence behind grids has been verified many times by different investigators. There have also been other laws developed similar to Taylor's, but none appear to have been an improvement.

A. A. Hall (14) has found that the accuracy of the mesh size is important, particularly if the decay of the turbulence is traced to low values. The lack of accuracy may lead to the production of eddies having a much larger scale than those corresponding to the mesh size owing to the existence of small cells which can couple with large cells several

mesh lengths away. In order to obtain the necessary accuracy, Hall found that the rods of the mesh should have the same diameter and that the resulting mesh be very accurately squared. These large eddies, which Cometta believed were caused by wall interference, will be of very low intensity and will therefore have no effect near the mesh, but owing to their slow rate of decay, they will become important when the total intensity of the turbulence has reached a low value.

A doubtful factor in the comparison between theoretical laws of decay of turbulence and experimental results is the extent to which turbulence initially present in the stream and wall-produced turbulence can interfere with turbulence produced by a mesh. For example, Hall obtained an increase of 10 to 20 per cent in u' with an increase in the initial turbulence from 0.2 to 1.3 per cent (15).

Isotropic turbulence decays with increasing distance from the turbulence producing sources. Typical results of the decay of isotropic turbulence behind square mesh grids were reported by Batchelor and Townsend (16), Corrsin (17), Simmons and Salter (18), Ducoffee (19), Baines and Peterson (20), Frenkiel (21), and others. The data indicated that the decay is essentially linear over a range of distances from the grid for $20 \leq \frac{x}{M} \leq 80$.

CHAPTER III

REVIEW OF THE LITERATURE - PART II

Measurement of Turbulence

In the preceding chapter turbulence and some of the theoretical relationships concerning turbulence, were discussed. In this chapter methods, instruments and techniques to measure such quantities as turbulence intensities, correlations, energy spectrums, probability densities, and various terms in the kinetic-energy balance and so forth, will be discussed.

The various methods, instruments and techniques may be divided into two groups for discussion. In the first group, a detecting element is introduced into the flowing fluid. The turbulence quantities are measured by the changes of a mechanical, physical, or chemical nature that occur in this element. This group will further be broken into instruments for gas and instruments for liquids. The instruments discussed which are used with gas are the constant-current and constant-temperature anemometer, and the glow discharge anemometer. The instruments discussed which are used in liquid are the hot-film anemometer, electromagnetic induction technique, and total head tube.

In the second group, a tracer or other indicator is introduced into the fluid to make the flow pattern visible or observable by a suitable detecting apparatus outside the field of flow. The instruments used in gas that will be discussed in this group are the electric spark and the shadow-graph. The ultramicroscope will be discussed as an instrument used in liquid.

Hot-Wire Anemometer

The hot-wire anemometer consists essentially of a wire of small diameter and short length placed in the air stream with its long dimension perpendicular to the direction of the mean flow and heated to a suitable temperature by means of an electric current. Fluctuations in the speed of the air stream produce fluctuations in the temperature of the wire and, hence, in its resistance.

Preliminary experiments on the use of a platinum wire heated by an electric current for the measurement of wind-velocity were carried out by G. A. Shakespear as early as 1902, but were discontinued for lack of facilities in the erection of a suitable whirling table for the calibration of the wires (22). Measurement of the current required to keep a wire at a given temperature as a method of measuring air velocity was independently suggested by A. E. Kennelly in 1909 (23). Electrical anemometry was also developed independently by J. T. Morris and U. Bordini about 1912. Actual measurements were carried out by Morris and Bordini (24). The above instruments were suited to the measurement of average velocities over a considerable area.

L. V. King in England in 1914 is given credit for first using the hot-wire technique for measuring the instantaneous velocity of moving fluids (22), (23). The special type of instrument developed by King was called a linear anemometer and consisted only of a single wire. It was especially suited for the study of turbulent flow and the analysis of sharp velocity gradients such as to be found in the neighborhood of obstacles in streams and in jets. An important application of this method is to be found in aerotechnical problems such as the analysis of propeller

wakes, distribution of velocities over planes of various dimensions and camber, etc. King's careful measurements and analysis furnished a firm foundation which had been lacking up to that time.

King's method has been used in several widely separated places and repeatedly modified. An important step forward was made by Mock and Dryden in 1932 (25). They used electrical networks to compensate for the reduced sensitivity and phase lag which introduced error in the response of the wire to higher frequency fluctuations.

Most of the earlier measurements used the constant-current anemometer. More recently, use has been made of the constant-temperature anemometer. These two methods will be discussed in the following material.

Constant-Current Anemometer

This method requires that the electric current I remain constant and that the temperature and, hence, the electric resistance change with fluctuating velocity.

The response of the hot-wire to a fluctuating air flow must be determined. Into the relation

$$\frac{I^2 R_w}{R_w - R_g} = A_2 + B \sqrt{U} \quad (2)$$

where A_2 and B are coefficients of hot-wire characteristics, R_w is the electrical resistance of the wire, R_g is the electrical resistance of the hot wire at gas temperature, and U is the Eulerian velocity, are introduced

$$U = \bar{u} + u \quad \text{and} \quad R_w = \bar{R}_w + r_w$$

where \bar{R}_w is the time-mean value and r_w is the electrical resistance of the turbulent fluctuation. If a low relative intensity of turbulence is assumed, the relation

$$e = Ir_w = -su = -\frac{(\bar{R}_w - R_g)^2}{2IR_g} B \sqrt{\bar{u}} \frac{u}{\bar{u}}$$

can be obtained where e is the voltage across the hot-wire and s is the sensitivity of the hot-wire.

The sensitivity of the hot-wire depends on the frequency of the velocity fluctuations owing to the finite thermal inertia of the hot-wire, and decreases for large values of frequency. There is a certain value called the time constant about which the sensitivity of the hot-wire becomes noticeable. The smaller the time constant, the higher the frequency of the velocity fluctuation to which the hot-wire may respond.

These relations apply to a wire with uniform velocity and temperature distribution along it and with no thermal effects. The response of the wire is, however, affected by the finite thermal inertia of the wire, the cooling action of the wire support, and the nonuniform velocity distribution along the wire.

The thermal inertia of the wire has a finite value causing a delay between the rapid fluctuations of the gas velocity and the corresponding temperature fluctuations of the wire. The thermal lag will cause the intensity of the turbulence to be too low, the microscale λ to be too high, and the dissipation to be too low. Dryden and others developed electronic compensation circuits for thermal inertia lag.

The wire supports are thick compared with the wire, so their temperature is practically equal to that of the ambient air. Because of the temperature difference between the wire supports, a cooling effect is exerted on the wire by conduction of heat to the support thus reducing the effective length of the wire.

In turbulent flow the velocity distributions are not uniform in regions down to the microscale of turbulence. Therefore, the wire should be as short as possible for making true "point" measurements.

Considering the effects of wire diameter, length, and length-diameter ratio, the acceptable sizes of wires range from 0.0025 to 0.005 mm in diameter and from 0.5 to 1 mm in length.

Constant-Temperature Method

In this method the electric resistance and temperature are kept constant as far as possible. By means of an electronic feedback system any slight variation in temperature and thus in electrical resistance due to the cooling effect of the turbulent-flow fluctuations, is compensated for. Much of the criterion for the use of the constant-temperature method is the same as the constant-current method so will not be discussed again.

There are certain definite advantages to the constant-temperature method which are:

- (1) The time constant at constant-temperature operation is much smaller than that at constant-current operation.
- (2) The thermal lag for most turbulent flows does not have to be compensated for.
- (3) The constants A_p and B in the equation

$$\frac{I^2 R_w}{R_w - R_g} = A_2 + B \sqrt{U}$$

are really constant.

(4) The signal-to-noise ratio is greatly reduced by the constant-temperature method.

(5) The error due to nonlinear temperature effect involved with high relative turbulence intensities, is reduced by a factor of roughly three by use of the constant-temperature method.

On the other hand, the electronic equipment required for the constant-temperature method is much more complicated than that used in constant-current operation.

The hot-wire anemometer has been used extensively by a great many investigators to study such things as turbulence intensity in three directions, correlations, energy spectrums, probability densities, the various terms in the turbulent kinetic-energy balance, and so forth (26). The material accumulated by these investigators is too much to be discussed in this study.

The hot-wire anemometer satisfies best the following requirements of a turbulence measuring instrument:

- (1) The instrument must be sufficiently strong and rigid to exclude vibrations caused by the flow.
- (2) The calibration parameters must not change during a test run.
- (3) The detecting element introduced into the flow must cause a minimum of disturbance.
- (4) The detecting element must be smaller than the dimensions of

the microscale of turbulence.

(5) The instrument must be sensitive enough to record small differences in the fluctuations.

(6) The inertia of the instrument must be low.

Glow Discharge Anemometer

The glow discharge offers possibilities for measuring turbulence in gases based on the potential-electric-current characteristics of an electric discharge between two electrodes. For electrodes of a given shape and gap, the characteristics depend on the nature, pressure, temperature, humidity and velocity of the gas.

F. C. Lindvall (27) developed an instrument with a minute glow discharge. This discharge at atmospheric pressure was characterized by a cathode glow a few thousandths of a centimeter in length and a potential difference of 300 volts and a positive zone having a voltage gradient of 1,500 volts per centimeter. The corresponding discharge current ranged from 10 to 30 ma. The total voltage across the electrodes was about 400 volts.

Lindvall found a useful working range for the gaps to be 0.010 to 0.025 cm. An extremely short gap was insensitive to air velocity while a long discharge was blown downstream into a bow shape having a greatly lengthened positive zone with corresponding abnormally high voltage.

The electrodes were 0.15 cm in diameter which was comparable to the dimensions of the glow itself. This was necessary so that the velocity, as measured, be definitely that of the stream flow and not the true velocity modified by the presence of bulky electrodes. The

electrodes were made of platinum because platinum gave a more consistently stable discharge as well as better reproducibility in data than did platinum-iridium or tungsten which were also tried.

This type of discharge was found to have agreement with the hot-wire anemometer when both were subjected to the well-known turbulence behind a cylinder in subsonic flow (28). Also, the electrical discharge had several advantages over the hot-wire anemometer, notably in calibration and simplicity of the amplifying equipment and the thermal time lag. The glow discharge had no lag in its response to air velocity change. The glow discharge had one outstanding defect because the electrical discharge will inevitably result in some slow loss of electrode material through sputtering and chemical modification in the presence of air.

Hot-Film Anemometer

S. C. Ling (29) in his Ph.D. Dissertation presented the original work using the hot-film anemometer which was very similar to the hot-wire anemometer.

The probe consisted of a thin platinum film fused on the wedge-shaped end of a glass or ceramic support. The support was prepared for the film by grinding, drawing, or otherwise forming it to the desired shape and dimensions. Wires for the electrical connections were imbedded in the support so that the platinum coating was the only metal exposed to the fluid (30). The hot-film anemometer has several superior mechanical characteristics which make it much better suited for measurements in liquids and high-temperature or supersonic flow of gases.

Ling and Hubbard (31) claim the wedge form minimizes the collection of microscopic dirt carried by the fluid and provides a more efficient and uniform heat-transfer surface. Heat transfer is concentrated at the front stagnation zone of the hot-film anemometer making it very sensitive to minute surface contamination in this area. The hot-film anemometer also has the advantages of a high signal-to-noise ratio and superior dynamic response. The high signal-to-noise ratio was contributed to several factors:

(1) The mechanical arrangement of the film supported by a glass or ceramic base eliminates extraneous signals due to stress and local vibrations which are present with the hot-wire anemometer.

(2) The thickness of the film can be varied at will to control the total resistance independently of its linear dimensions. The dynamic response of the hot-film anemometer was very good at high frequencies, but at low frequencies it did not respond well.

Electromagnetic Induction

This method of investigating the flow of liquids has the advantage of using the very simple and universally valid relation which exists between the velocity and the induced electromotive force. Since the electromotive force is induced instantaneously and depends upon the direction of the velocity as well as its magnitude, the method can differentiate between motions in different directions and can represent velocity-alterations of high frequency as well as those of low frequency (32).

The physical principle upon which the experimental method was

based was Faraday's law of electromagnetic induction which indicates that electromotive forces are induced in a liquid conductor moving relative to a magnetic field. If U is the velocity component perpendicular to an electromagnetic field with strength H , and V is the strength of the induced electric field, then

$$V = \frac{a}{c} HU$$

where a is the relative magnetic permeability of the liquid and c is the velocity of light (33).

Grossman has developed a useful technique for determining the RMS turbulent-velocity fluctuations, the Reynolds stresses, and the Lagrangian velocity correlations (33), (34). He developed a probe of sufficiently small electrode spacing that could be arranged to traverse the flow field to yield the distribution and character of the velocity components. Grossman's flow system consisted of a 30 foot long, 1.732 inch inside diameter Lucite pipe fed from a constant head tank and discharging into another tank provided with overflow head control. The liquid used was water. A steady magnetic field was produced by a direct-current electromagnet.

This method has the disadvantage that the quantity measured directly by experiment is the difference in potential between two points in the liquid and not the emf, and these are not equal due to the flow of currents existing in a liquid of finite conductivity by virtue of the induced electric field. These currents are not dependent on the velocity, but on the velocity gradients, and not on the local conditions, but on the entire field.

The magnitude of the background noise varied from 10 to 100 per cent of the induced signal, but a method was worked out to correct this.

The method of electromagnetic induction has the advantage of being independent of such physical parameters as pressure, density, temperature, composition, electrical conductivity, etc. This method does not have the problem of thermal lag, and the necessary compensation circuits familiar in hot-wire anemometry.

Total Head Tube with Ceramic Pressure Transducer

The earlier work with this type of turbulence probe in water was done by Ippen (35), Ruetenik (36), and Perkins (37). This particular probe discussed below is the one used by Eagleson and co-workers (38). Eagleson's probe is discussed here because it is essentially the same as the other probes except that it embodies the latest improvements in this type of instrument.

In order to measure the turbulence characteristics, a traversing system with a strut going completely through the pipe was developed. This streamlined strut contained three probes for the measurement of total head, static pressure and turbulent pressure fluctuations.

The total head tube used in the transversing strut was a standard Pitot-static tube. Actually, only the total head was measured with the Pitot-static tube because theoretical calculations showed that an error of about 6.5 per cent was introduced into the measured mean velocities if this tube was to be used to measure static pressure. The actual error involved in measuring the static pressure with the Pitot-static tube was 5 per cent.

A static pressure probe separate from the total head tube was designed in order to procure the desired measurements in the immediate vicinity of the trailing edge of the test plates. The static pressure probe showed an error of only 2 per cent over the entire range of tunnel operation.

A total head tube with a circular disc-shaped barium titanate ceramic pressure transducer 0.125 inch in diameter and 0.10 inch thick was developed to assist in the experimental approach to the study of turbulence in the flow of water. The crystal was placed in a "cup" which plugged into a coaxial cable which formed an electrical connection by pressure contact between the silvered faces of the crystal and the silver-plated plug and silver-plated external diaphragm. A low capacitance cable was used and was kept as short as possible.

Because of the large ceramic transducer and the mounting arrangement, a liquid filled nose cone which tapered down to 1/16 inch diameter for "point" measurements was added forward of the crystal. The nose cone of the turbulence probe fitted over the tip cover and was made airtight by a thin layer of sealing wax.

The instantaneous response of a total head tube aligned with the direction of mean flow is given by:

$$H_{tg} = \frac{\bar{p}}{\gamma} + \frac{p'}{\gamma} + \frac{(\bar{u} + u)^2}{2g}$$

This equation assumes that velocity components perpendicular to the mean flow have no effect and that the length scale of the turbulence is large compared to the diameter of the probe tip. The turbulence probe was also insensitive to mean quantities because of its low frequency responses.

The output of the probe is

$$H_{tg} = \frac{p'}{\rho} + \frac{\overline{uu'}}{\rho} + \frac{u'^2}{2\rho}$$

A disadvantage of the probe is its indiscriminate response to pressure fluctuations of any variety including those of acoustical origin. The probe also does not respond to static pressure changes, consequently limiting its use for pressure measurement. Because of the water-filled nose cone, the high natural frequency of the crystal, due to the inertia of the liquid therein, was reduced to 10,000 cps.

The relative turbulence intensity due to free stream flow conditions, ranged from 5.7 per cent to 7.8 per cent which was rather high. Perkins (37) indicated a turbulence level in the same water tunnel of only 2.8 per cent. The reason for the higher turbulence level was explained by the difference in the probes used. The probe developed by Eagleson and co-workers (38) measured a large amount of energy at the low frequencies which could have an appreciable effect on the determination of turbulent intensity. In some cases the turbulence intensity tended to increase in the downstream direction which was unexpected because viscous decay of the small scale turbulence introduced by the grids should cause a decrease in intensity in the downstream direction.

The spectra of the longitudinal turbulence energy was the general form of the spectra obtained in air. However, it was noted that $\int_0^\infty E(n) \, dn$ should have been equal to $\overline{u^2}$ if all the energy was recorded in the measured energy spectrum. $E(n)$ is the spectral distribution function of longitudinal turbulence kinetic energy density per unit mass

in ft^2/sec^2 cps. But $\int_0^{\infty} E(n) \, dn$ was not equal to u^2 , so the 25 per cent of the unrecorded energy must be in the spectra from 0 to 2.5 cps or possibly above 750 cps which was the upper limit on the wave analyzer employed in Eagleson's work.

Electric Spark

Townsend (39) developed a method of measuring the turbulent components of the velocity in a stream of air by producing a spark between very fine electrodes situated at a point in the flow which heated small elements of air in its immediate neighborhood. By means of the Schlieren method of photography, this hot spot of air could be made visible and its subsequent motions photographed. The ability to produce a regular series of identifiable elements of the fluid provided the opportunity of measuring the values of u , v , and w as well as their maximum values. The velocity distributions across the pipe were studied by placing a row of seven spark gaps across the pipe.

Cinematograph records were made which could be analyzed to obtain the mean velocity and the three components of the deviations from the mean velocity due to turbulence at any point in the stream. At each point the velocities were derived from a film having about 200 pictures. This was a cumbersome process and involved a great deal of labor.

The accuracy with which the position of the hot spot could be read from the film was rather low because the image of the spot was ill-defined and the spot was often rapidly distorted and sometimes broken up into two or more discrete fragments. However, the errors probably canceled where large numbers of spots were measured.

The maximum values of u , v , and w measured by an electric spark compared favorably with u_1 , v_1 , and w_1 measured by the ultramicroscope which will be discussed later. It was also found that the maximum value at any point was roughly three times the RMS value of the turbulent components or 3.75 times the average value. A distribution of turbulence was found to be a minimum near the axis and a maximum near the walls which agreed with the measurements made by the ultramicroscope.

Shadowgraph

Kovasznay (40) has devised a method of obtaining information concerning the turbulence structure from a refraction image. The shadowgraph method was developed because the hot-wire anemometer could not measure the frequency responses of high subsonic and supersonic speeds.

The most obvious limitation of the hot-wire method is the thermal capacity of the wire itself. By suitable electronic compensation, the hot-wire anemometer can measure frequencies on the order of 10,000 cps. This corresponds to a wavelength of the order of an inch whereas, in supersonic flows, the wave lengths are much smaller.

The shadowgraph method is an optical method. There are two main objections to the use of any type of optical method:

- (1) There is no point-to-point relationship between the picture obtained and the three dimensional flow.
- (2) The optical method gives information only about density fluctuation.

However, the shadow method responds to second derivatives of the density fluctuation, so therefore has the greatest prospects of resolving

very high frequency components of turbulence.

If parallel incident light is assumed and the turbulent region deflects the light randomly, then small density disturbances in the turbulence field act as small convex or concave lenses that turn the parallel light into convergent or divergent beams. Hence, the light arriving at the photographic plate will be more or less intense than the original parallel light according to the distortion. If two transparent pictures are made from the shadowgraph and placed face to face, the combined pattern is the same as for the single plate if there is complete coincidence of the pictures. If the pictures are shifted a little with respect to each other, a decrease in transparenence is obtained. Now the resultant transparenence of the two pictures is equal to the product of the transparencies of each individual picture. This fact offers the possibility of determining the correlation between densities at two neighboring points of the flow field.

Hinze (2) has derived an expression for the relation between the turbulent component of velocity and the density of the fluid. Therefore, a correlation between density variations must be identical to a correlation between corresponding turbulence velocities at two points, hence, this method offers a means of measuring the velocity correlation.

Kovasznyay found that the scale of turbulence measured was very small thus indicating that the corresponding frequency would be of the order of a few hundred kilocycles. He found that the shadowgraph method does not give good measurement of the turbulence level but does give better resolution in spatial statistical properties at high velocities

than do previous methods.

Ultramicroscope

Fage and Townend (6) developed a method using the ultramicroscope to study microturbulence. Previously, turbulent fluid had been studied by introducing particles of extraneous matter such as aluminum particles, oil drops, etc., into the flow. Fage and Townend reasoned that if the particles introduced were comparable in size with the molar masses, their internal motions may not be correctly represented. Therefore, it was desirable to avoid any such interference with the flow. The ultramicroscope offered a means of doing this.

The principle of the ultramicroscope depends on the fact that minute particles can become visible as bright points of light when intensely illuminated against a drab background.

The experiments were made on the flow in a square brass pipe and in a circular pipe. A uniform flow of tap water through the experimental pipe was maintained by means of a constant difference of head between water levels in the supply and exhaust tanks. A special pump was designed so that rust or dirt, inevitable with an ordinary pump, would not be present in the system.

Reliable observations with the ultramicroscope of the maximum values of the angular deviation of flow in the horizontal plane and in the vertical plane (denoted by Θ_{xy} and Θ_{xz}) and of the instantaneous velocity (denoted by u_1), at any point in the fluid were obtained except near the boundary. The ultramicroscope was not capable of obtaining continuous records of the variations of the velocity components

with time or their deviations of flow from the mean flow. The maximum value of the components of the velocity disturbance v_1 , and w_1 could be deduced from the observations if use was made of the relationship

$$v_1, w_1 = (\bar{u} + u) \tan (\theta_{xy}, \theta_{xz})$$

The angular deviation of flow, which showed as an illuminous streak, was measured by means of a fine platinum wire mounted in the focal plane of the eyepiece. To facilitate observation the wire was rendered luminous by electrically heating it to a dull red glow. Observations showed that the flow along the axis of either pipe was more disturbed over the critical range of Reynolds numbers than either above or below it. The Reynolds number used here was $\frac{\bar{u}m}{\nu}$, where m is the hydraulic mean depth. When turbulence was fully established, the value of the angular deviation of flow was not greatly influenced by a change of Reynolds number. This indicated that there was no growth in the degree of turbulence.

A method based on the principle that a microscope moving at the same speed as a particle would make it appear as a bright stationary point instead of a streak was used to observe the maximum deviations u_1 from the mean speed. Instead of moving the microscope, the same view could be obtained if the eyepiece and the microscope tube were fixed relatively to the pipe and the objective only was moved in the same direction as the particle. If at the instant of observation the velocity components due to the moving objective were the same as those of a particle, that particle would appear as a point; likewise, if the objective

was moving with an effective speed equal to $(\bar{u} + u)$, the particle would appear as a short streak. The value of $(\bar{u} - u_1)$ could be obtained by slowly increasing the speed of the microscope until "stationary" particles first appeared, and the value of $(\bar{u} + u_1)$ could be obtained by increasing the speed further until they just ceased to appear. It was found that the greatest velocity fluctuations occurred in a cylindrical region of the fluid approximately midway between the centerline and side of the pipe. It was also found that near the center of the pipe the ratios u_1/\bar{u} , v_1/\bar{u} , and w_1/\bar{u} were approximately equal; but as the wall was approached, the ratio v_1/\bar{u} obtained from the velocity disturbance normal to the wall decreased to zero while the other two ratios u_1/\bar{u} , and w_1/\bar{u} increased. No information about the mean turbulence could be obtained.

Fage and Townend (39) performed further experiments with the ultramicroscope at much higher Reynolds numbers. The evidence in this work supported the results obtained in their earlier work (6).

CHAPTER IV

EXPERIMENTAL APPARATUS

Figures 2 and 3 show the experimental flow system consists of a constant head tank, head bay, contraction cone, square mesh grid, test section, and a tail water bay. This system was designed by Dr. P. G. Mayer and built in the Georgia Tech Hydraulics Laboratory.

Flow through the test section was controlled by maintaining a constant water surface elevation between the two tanks and manipulating the valve at the downstream end of the system. The required discharge was determined by an elbow meter located between the constant head tank of the laboratory and the head bay of the water tunnel.

Both the head bay (8 feet long, 4 feet wide, and 4 feet deep) and the tail water bay (4 feet cubed) were made of $3/4$ inch plywood and lined with fiberglass. The entire system was supported on eight 2 x 4 inch legs approximately 2 feet tall.

The test section consists of an 8 inch inside diameter plexiglass tube 50 inches in length. Both the entrance and outlet to the test section were fitted with a bell-shaped contraction cone made of fiberglass. A $1/2$ inch square mesh grid with $1/16$ inch diameter wire was placed at the upstream junction of the tube and the contraction cone.

Five test sections numbered one to five from the head bay were located at distances of 2.125, 12.25, 22.125, 32.25, and 42.25 inches downstream from the grid. Both the turbulence probe and the velocity tube were inserted through stuffing box fittings located on the top of the test section.

The Contracting Cone

In designing a contracting cone for a wind tunnel the geometric form of the cone must be such that a uniform velocity distribution is obtained at the tunnel entrance. However, if the velocity at the end of the contraction cone is about 0.9 that of sound, the danger of compressibility shock occurs. This danger can be avoided by keeping the velocity in the contraction cone below that of sound. The highest velocity is reached at the wall of the cone. Therefore, if the velocity at the wall is made to increase monotonically from the beginning of the cone to the end, the velocity in the cone will always be less than that of sound provided the velocity at the entrance to the tunnel is less than that of sound. Also, if the curvature of the wall of the contraction cone is too large at certain points, local velocities at these points may exceed the uniform velocity at the end of the contraction cone causing an adverse pressure gradient and, perhaps, boundary layer separation from the wall. However, with a monotonically increasing velocity the pressure along the wall will be decreasing monotonically and the danger of boundary layer separation is avoided (41).

For the water tunnel, the anticipated velocities were very much less than the speed of sound. The coordinates of the axisymmetric contraction cone are given in Table 3. The distance from the P. T. is designated X , and the radial distance by r (42). A photograph of the contraction cone is given in Figure 4.

Test Tunnel

In designing a water tunnel the turbulence created at the walls and diffused into the main stream must be kept at a minimum. This means

that the boundary layer in the water tunnel must not interfere with the turbulence structure behind a grid if the turbulence measurements are to be used for comparison with other studies. Therefore, the test tunnel was designed so that it could have a satisfactory portion of the cross section of the 8 inch inside diameter pipe free of interference from turbulence created at the pipe walls.

Since most studies of boundary layer growth were conducted in air, a corresponding Reynolds number of a similar tunnel would depend essentially on the ratio of the kinematic viscosities.

To estimate the boundary layer growth in water, it was assumed that the ratio δ/D was small and that the test section would behave approximately as a flat plate.

Boundary layer growth on a flat plate in turbulent flow is expressed by:

$$\delta/x = .377 \left(\frac{\nu}{u_x} \right)^{1/5} \quad (4)$$

The values of Table 2 (based on 68°F) indicate that the mean velocity of 1.5 ft/sec will generate a boundary layer thickness of about 2 inches at a distance of approximately 7 feet from the leading edge. Therefore, a test tunnel 50 inches long should provide a sufficient portion of the cross section for the study of isotropic turbulence.

Pitot-Static Tube

A standard pitot-static tube was used to measure the mean velocity at the centerline of the pipe and to measure the velocity profiles across the pipe.

Velocity profiles were taken at all five longitudinal stuffing box stations for three different pipe Reynolds numbers which were $.616 \times 10^5$, 1.07×10^5 , and 1.68×10^5 .

Turbulence Probe

The turbulence probe used in these tests was developed by George F. Smoot of the United States Geological Survey (43). It consisted of a 1.4 inch diameter L shaped tube with a one-mil-thick beryllium-copper diaphragm mounted on the tip. A four arm strain gage bridge of a special design was bonded to the inner surface of this diaphragm. This transducer was used in conjunction with Sierra Electronic Corporation Model 188 carrier power supply and Model 114 carrier amplifier.

It is well known that a thermocouple voltmeter is the most accurate means of measuring the root-mean-square value of a random electronic signal. Therefore, a Sensitive Research Instrument Corporation's Model A thermocouple voltmeter was chosen. Caution had to be exercised in using an instrument of this type to filter any D. C. components out of the signal, as the thermocouple was unable to discriminate between A. C. and D. C. voltages. To eliminate the D. C. portion of the signal, a filter was designed to cut off the extreme low frequencies (below about 2 cycles per second).

To provide the necessary power for the thermocouple voltmeter, a Tektronix, Inc., Type 133 power supply unit with a Type A wide-band D. C. preamplifier was used. This unit served both as a cathode-follower and as an additional amplifier.

A General Radio Type 1554-A Sound and Vibration Analyzer was used to determine the mean energy spectrum. This analyzer had a frequency

range of 2.5 to 2500 cycles per second.

This equipment was not accessible to the writer, but some tests were carried out previously in the Georgia Tech tunnel by personnel of the United States Geological Survey. The turbulence measurements made by the personnel of the United States Geological Survey were used in conjunction with the measurements obtained by the writer.

CHAPTER V

EXPERIMENTAL PROCEDURE

Baffling

In order to have isotropic turbulence in a pipe, it is necessary to have a uniform velocity profile in a flow initially free of turbulence on which to superimpose the generated turbulence.

Large eddies were created as the water discharged from the constant head tank into the head bay. The inflow was directed toward the back wall of the head bay. These eddies created swirls and distorted the velocity profiles in the test tunnel.

In order to eliminate eddies in the head bay, large rolls of wire mesh of two different sizes were placed beside the discharge pipe and at different locations in the head bay along with a floating wooden grid (see Figure 2) to facilitate eddy break-up. Red dye was used to facilitate placing these wire rolls so that the eddies could be eliminated.

Mean Velocity Calibrations

It was first thought that the mean pipe velocities plotted as a function of the manometer elbow meter deflection would produce a different curve for each of the five stations because of boundary layer growth and that these curves would be increasing in magnitude as succeeding stations downstream were calibrated. However, this was found not to be the case. Mean velocities as a function of elbow meter manometer deflections for all five stations were found to plot on one curve. Points for the curve

were taken for manometer deflections varying from 0.1 feet to 3 feet giving a variation in mean velocity of 0.4 ft/sec to 2.7 ft/sec as can be seen in Figure 5. This curve was also used in conjunction with the turbulence components of velocities measured by the United States Geological Survey personnel.

Profile Velocity Calibrations

The primary purpose of measuring the velocity profiles was to determine the degree of uniformity of flow in the test tunnel. Only if the pipe flow consists essentially of uniform flow is it possible to have isotropic turbulence. Velocity profiles were taken for pipe Reynolds numbers of $.616 \times 10^5$, 1.07×10^5 , and 1.68×10^5 at all five stations. The measurements were made with a pitot-static tube. Readings could be obtained to the nearest one-thousandth of an inch.

Turbulence Behind a Grid

Isotropic turbulence was generated behind a grid with bar sizes of 1/16 inch diameter and mesh sizes of 1/2 inch placed at the end of the entrance contraction cone. The RMS values of velocities were measured by the United States Geological Survey at stations 2 and 4 along the center line of the pipe. The ratio u' to the mean velocity \bar{u} is plotted against mesh Reynolds numbers in Figure 9 which shows the trends and the magnitudes of the u' component. The decay of turbulence behind the grid is illustrated by plotting $(\frac{\bar{u}}{u'})^2$ against $\frac{x}{M}$ in Figure 10. Some reference data are also shown for comparison.

CHAPTER VI

DISCUSSION OF RESULTS

Tunnel Calibrations

The results of the tunnel calibrations are shown in Figure 5 as a plot of manometer deflections (from the elbow meter) versus indicated velocity (from the pitot-static tube). The data shown are for the longitudinal stations 1, 2, 3, 4, and 5. As was mentioned in Chapter V, it was first thought that a different curve for each of the five stations would result. As the boundary layer grows, continuity considerations require that the fluid in the center of the pipe accelerates, thus, increasing the mean or centerline velocity which in turn ought to cause curves of progressively longer magnitude to develop as succeeding stations downstream are calibrated. However, this was not the case. The data points for a particular manometer deflection setting were sufficiently close to indicate that a single curve could be used for setting the speed at any stuffing box station without introducing appreciable error (19).

A great deal of trouble was encountered in finding a fluid to give sufficient deflection in the pitot-static tube. A Meriam manometer fluid of specific gravity 2.94 was finally used.

Velocity Profiles

The velocity profiles obtained from pipe Reynolds numbers of $.616 \times 10^5$, 1.07×10^5 , and 1.68×10^5 can be seen in Figures 6, 7, and 8 respectively. Although there were small variations in the velocity profiles which were due to difficulties with the fluid in the pitot-static

tube, the velocity profiles indicated uniform flow at each succeeding downstream station. The variations were random. A theoretical plot of the growth of the turbulent boundary layer on a flat plate has been included in these figures since the flat plate criterion had been used in the preliminary design. From Figures 6, 7, and 8, it can be seen that the flat plate criterion was a reasonable assumption and that a tunnel 50 inches long is satisfactory for the study of isotropic turbulence. These profiles indicate that the entrance conditions are very good and that isotropic turbulence can be expected in the center portion of the tunnel cross section.

Turbulence Behind Grids

The ratio of the RMS value u' to the mean velocity \bar{u} is plotted against the mesh Reynolds numbers in Figure 9 and shows the general trends and the magnitudes of the u' component. This figure shows that the turbulence is in correct order of magnitude.

The decay of turbulence behind the grid is illustrated by plotting $(\bar{u}/u')^2$ against x/M in Figure 10. By comparing the results of other investigations, it is seen that the decay rate is much smaller than was expected from isotropic turbulence. A definite trend is observed, for it can be seen that as the mesh Reynolds number increases, the decay curves tend to become steeper and approach the work of other investigators.

The mean energy spectrum was measured and plotted (43). It showed that the general trends were sound. However, the scatter of points at low frequency was large and it was not feasible to compute the correlation coefficient from the mean energy spectrum by the

formula

$$R = \int_0^{\infty} F(n) \cos \frac{2\pi n x}{u} dn$$

Because the background noise was not measured, the area covered by the energy spectrum was not equal to unity as it should be according to the formula

$$\int_0^{\infty} F(n) dn = 1$$

The initial turbulence levels were not measured in the head bay and the approach section. The deviation from wind tunnel results may be caused by free stream turbulence initially in the system. As the mesh Reynolds number is increased, the superimposed turbulence due to the grid is increased in magnitude and tends to overshadow the free stream turbulence. However, this has not been verified because the United States Geological Survey did not measure the turbulent intensities without the grid. The United States Geological Survey also had trouble with the noise level due to external vibration of the test system, with reading the RMS voltages, and with pressure fluctuations from the tail box. All of these could have contributed to turbulence intensity measurements in these tests.

CHAPTER VII

CONCLUSIONS

From the calibrations and turbulence measurements obtained in this investigation, the following conclusions can be drawn for the performance of the water tunnel.

(1) The velocity profiles indicate uniformity, a condition necessary but not sufficient for the presence of isotropic turbulence.

(2) The magnitude of u'/\bar{u} versus R_m was in the right order of magnitude when compared to wind tunnel tests.

(3) The decay of isotropic turbulence was less than expected when compared to wind tunnel tests.

(4) The mean energy spectrum showed that the general trends were sound.

(5) This water tunnel can be used as a calibrating device for turbulence probes provided a few alterations which are mentioned in Chapter VIII, are made.

CHAPTER VIII

RECOMMENDATIONS

The writer feels that further tests of this type should be performed with certain modifications. These modifications are:

(1) An improved instrument for measuring turbulence in water is needed. The instrument should be able to measure higher as well as lower frequencies than the present total head tube. When this is available, the turbulence intensities, correlation functions, and energy spectrums should be measured over a greater range of discharge Reynolds numbers.

(2) The free stream turbulence without a grid should be measured.

(3) The grid should be precisely made for the reasons given in reference 14.

(4) Various grid sizes should be tested. The values of M/d from 3 to 11 are suggested.

(5) The decay of turbulence should be determined at all five stuffing box stations.

(6) The tail bay should be enlarged and reinforced so that pressure fluctuation is reduced to a minimum.

(7) The test system should be placed on a more rigid foundation so that vibrations are reduced.

APPENDIX

Table 1. Cone Coordinates

x, ft.	r, ft.
0.0	0.333
0.2	0.333
0.4	0.337
0.6	0.351
0.8	0.374
1.0	0.443
1.2	0.519
1.4	0.615
1.6	0.729
1.8	0.859
2.0	1.009

Table 2. Boundary Layer Growth

X, ft	\bar{u} ft/sec	\bar{u} ft/sec
	for $\delta = 1"$	for $\delta = 2"$
1	0.02	0.0006
2	0.33	0.01
3	1.66	0.05
4	5.25	0.16
5	12.81	0.40
6	26.62	0.82
7	49.30	1.52
8	84.00	2.60

Table 3. Turbulence Intensities

Run No.	Man. Def.	\bar{u}	u'	$\frac{u'}{\bar{u}}$	$(\frac{\bar{u}}{u'})^2$	$\frac{\bar{u}M}{\nu} \times 10^{-4} *$	Sta. No.	$\frac{x}{M}$	$\frac{x}{d}$
11	0.760	1.34	.0390	.0291	1119	.559	2	24.5	196
12	1.400	1.77	.0403	.0228	1927	.739			
13	0.472	1.08	.0375	.0347	831	.451			
14	0.295	0.85	.0335	.0394	645	.355			
15	1.082	1.58	.0371	.0234	1823	.660			
16	0.114	0.50	.0369	.0739	183	.209	2	24.5	196
17	0.112	0.49	.0410	.0837	143	.204	4	64.5	516
18	0.302	0.86	.0445	.0517	374	.359			
19	0.462	1.07	.0446	.0417	575	.447			
20	0.770	1.35	.0448	.0332	907	.564			
21	1.105	1.59	.0394	.0248	1628	.664			
22	1.430	1.79	.0423	.0236	1797	.748			
23	3.220	2.77	.0503	.0182	3020	1.157			
24	1.100	1.59	.0421	.0265	1423	.664			
25	0.469	1.07	.0424	.0396	637	.447	4	64.5	516
26	0.482	1.09	.0476	.0436	524	.455	2	24.5	196
27	0.296	0.85	.0483	.0569	309	.355			
28	1.080	1.32	.0503	.0381	688	.552			
29	3.160	2.74	.0699	.0255	1538	1.144	2	24.5	196

*Assume an average of the temperatures to calculate the kinematic viscosity. $T = 74.4^\circ\text{F}$ $\nu = .997 \times 10^{-5}$

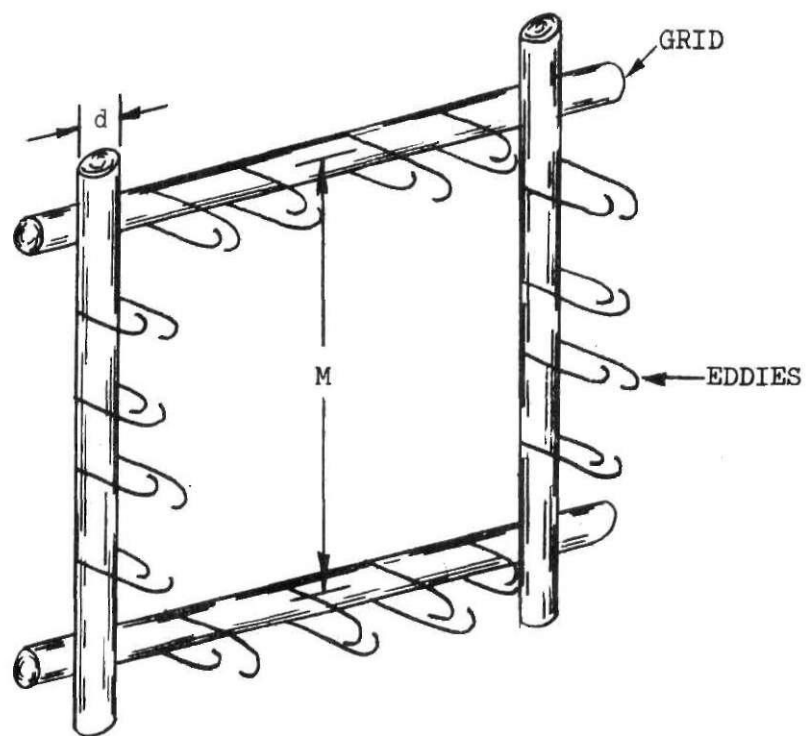


Figure 1. Grid Forming Isotropic Turbulence

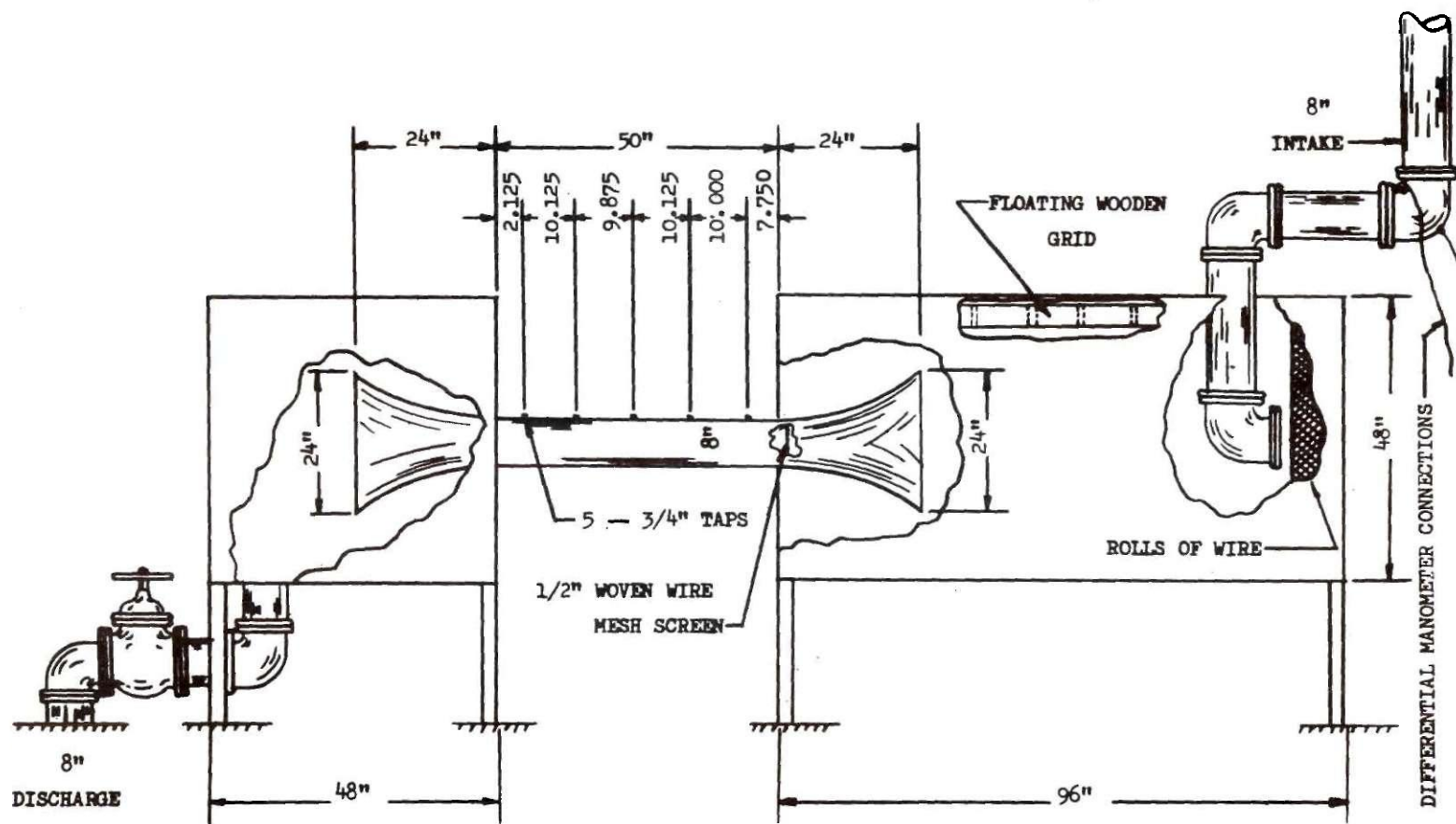


Figure 2. Side View of Water Tunnel

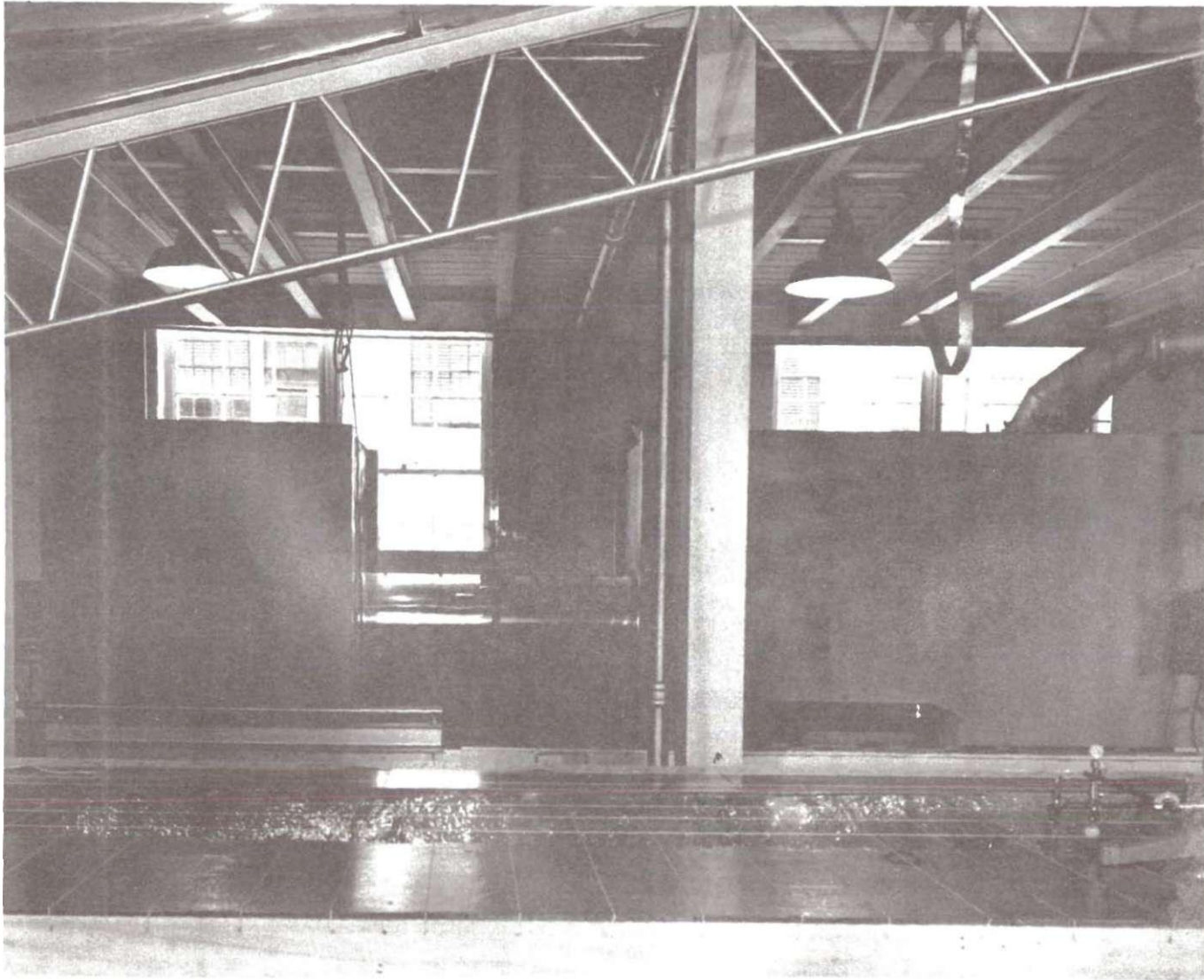


Figure 3. Photograph of Water Tunnel

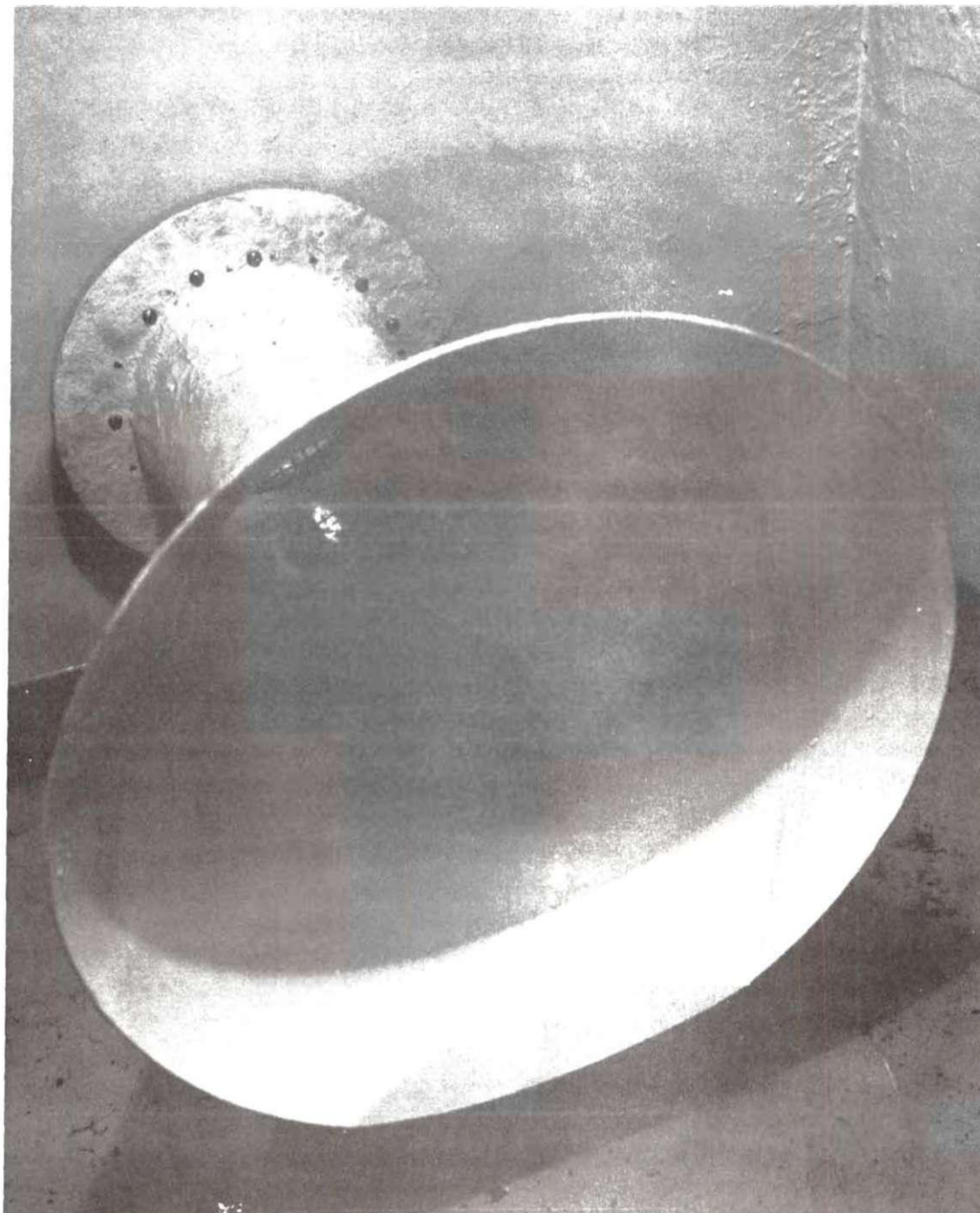


Figure 4. Photograph of Contraction Cone

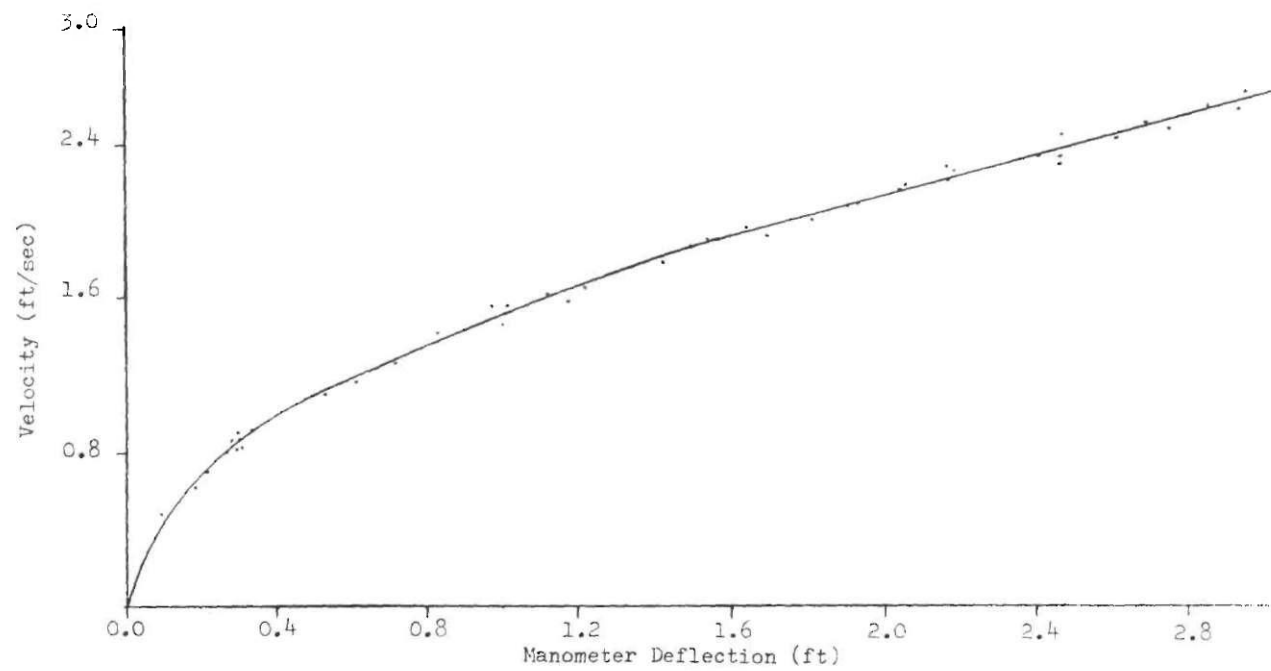


Figure 5. Velocity - Discharge Relationships

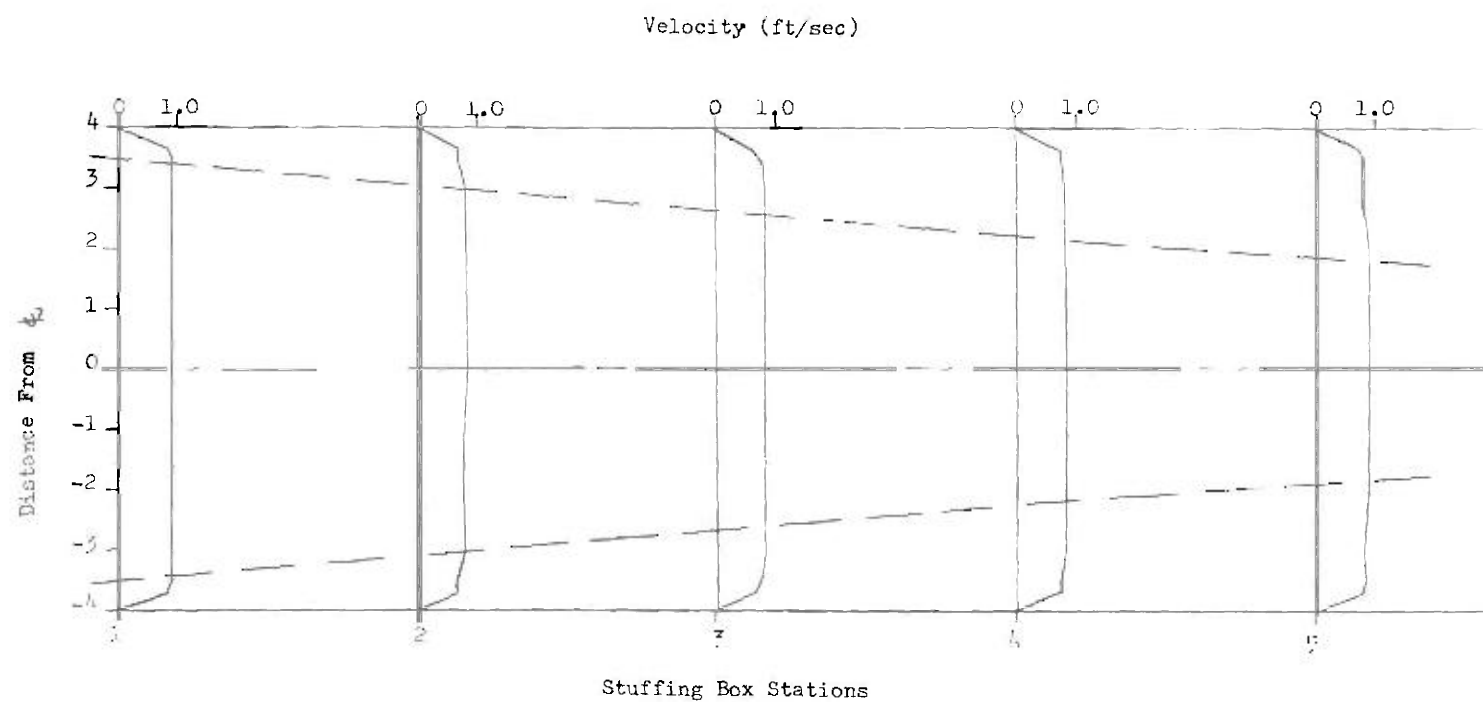


Figure 6. Velocity Profiles at $R_p = .616 \times 10^5$

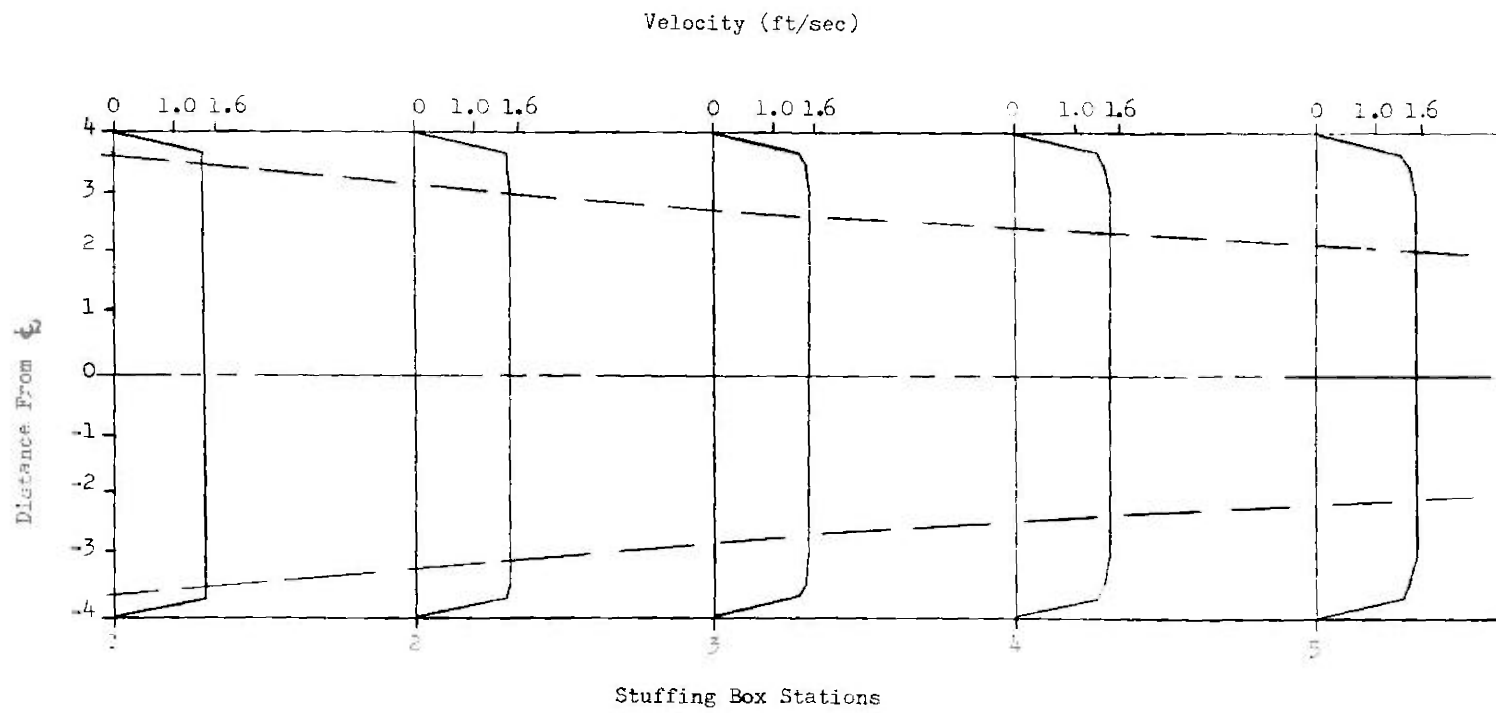


Figure 7. Velocity Profiles at $R_p = 1.07 \times 10^5$

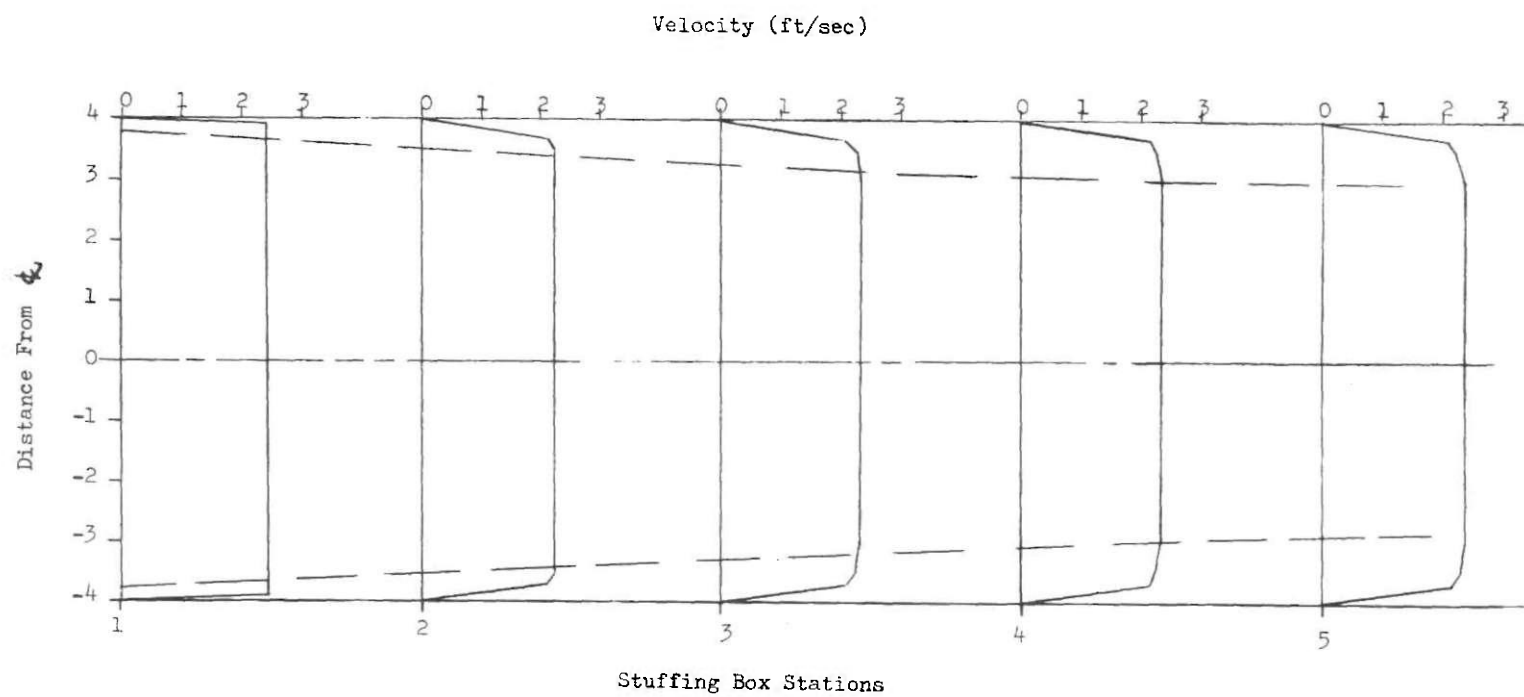


Figure 8. Velocity Profiles at $R_p = 1.68 \times 10^5$

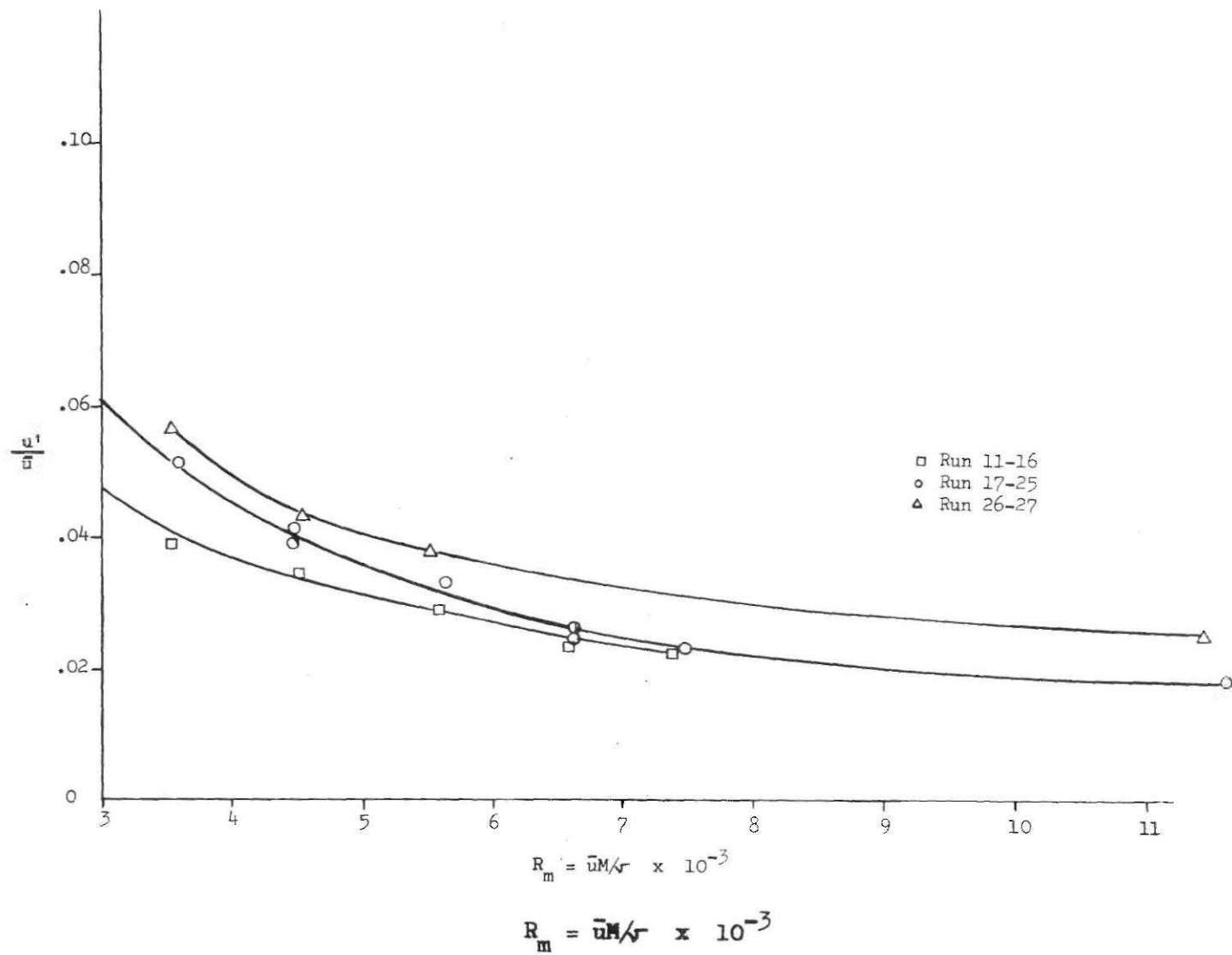


Figure 9. Turbulence Intensity

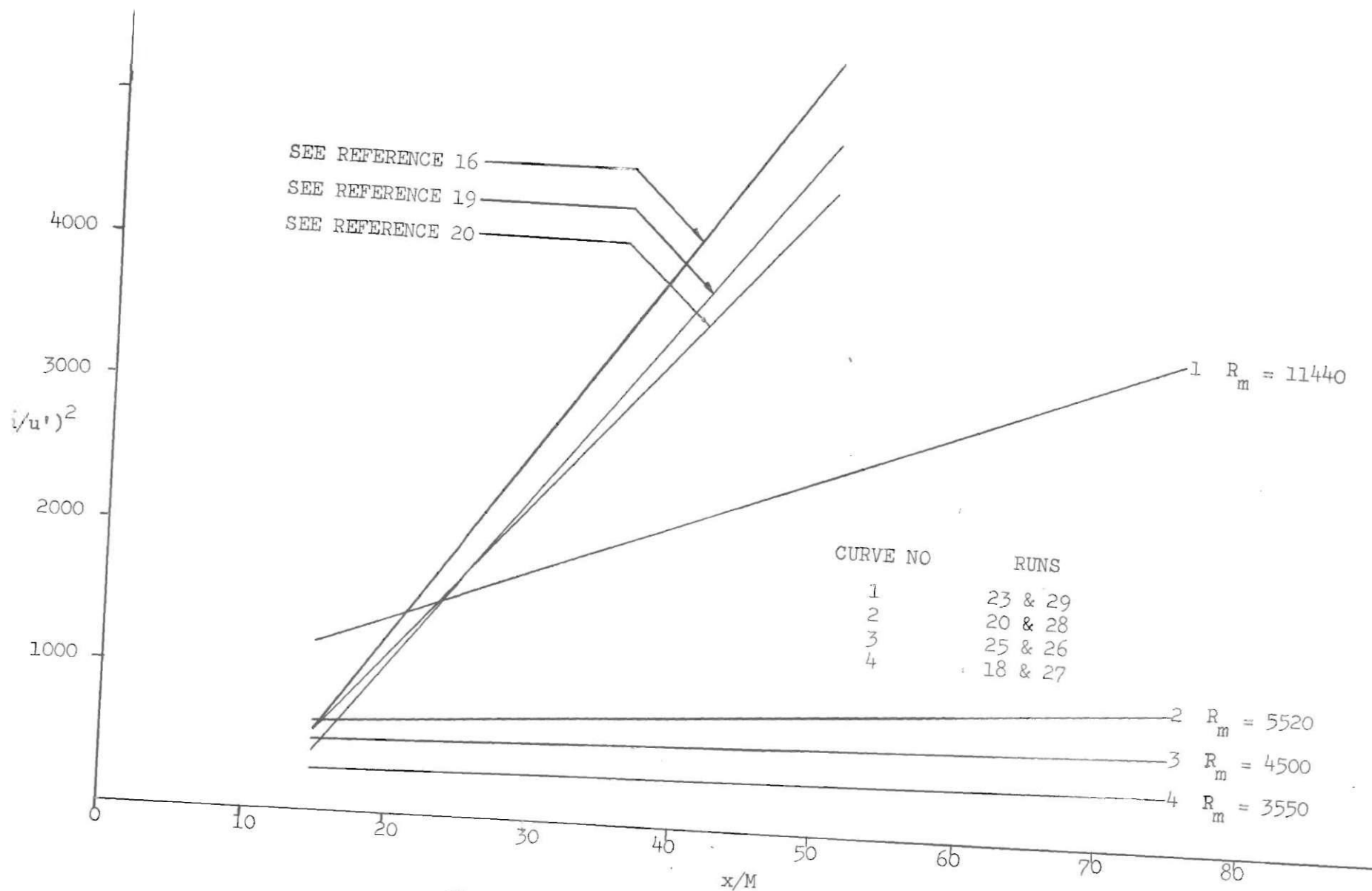


Figure 10. Decay of Grid Turbulance

BIBLIOGRAPHY

1. Vennard, J. K., Elementary Fluid Mechanics, 4th Edition, Wiley and Sons, 1961.
2. Hinze, J. O., Turbulence, McGraw - Hill, 1959.
3. Rouse, H., Engineering Hydraulics, Wiley and Sons, 1960.
4. Rouse, H., Elementary Mechanics of Fluids, Wiley and Sons, 1960.
5. Schlichting, H., Boundary Layer Theory, 4th Edition, McGraw - Hill, 1960.
6. Fage, A., and Townend, H. C. H., "An Examination of Turbulent Flow with an Ultramicroscope," Proceedings of the Royal Society of London, Series A, Vol. 135, 1932, p. 656.
7. Taylor, G. I., "The Spectrum of Turbulence," Proceedings of the Royal Society of London, Series A, Vol. 164, 1938, p. 476.
8. Karman, von T., and Howarth, L., "On the Statistical Theory of Isotropic Turbulence," Proceedings of the Royal Society of London, Series A, Vol. 164, 1938, p. 192.
9. Bennett and Lee, "On Experimental Study of Boundary Layer Transition," American Society of Civil Engineers Transactions, Vol. 122, 1957, p. 307.
10. Goldstein, S., Modern Developments in Fluid Dynamics, Oxford, Vol. I, 1938, p. 299.
11. Pai, Shih - I, Viscous Flow Theory II - Turbulent Flow, D. Van Nostrand Co., Inc., 1957.
12. Cometta, C., "An Investigation of the Unsteady Flow Pattern in the Wake of Cylinders and Spheres Using a Hot-Wire Probe," OSR-TN-57-760, 1957.
13. Taylor, G. I., "Statistical Theory of Turbulence," Proceedings of the Royal Society of London, Series A, Parts I-IV, No. 823, Vol. 151, 1935. Part V, No. 888, Vol. 156, 1936.
14. Hall, A. A., "Measurements of the Intensity and Scale of Turbulence," R & M, No. 1842, Aeronautical Research Committee, Great Britian, 1938.

15. McNown, J. S., and Albertson, M. L., "Review of Experimental and Theoretical Studies of Flow Behind Grids," Iowa Institute of Hydraulic Research Memorandum, October 1945.
16. Batchelor, G. K., and Townsend, A. A., "Decay of Vorticity in Isotropic Turbulence," Proceedings of the Royal Society of London, Series A, Vol. 190, 1947, p. 534.
17. Corrsin, S., "Decay of Turbulence Behind Three Similar Grids," California Institute of Technology, Pasadena, California, 1942, (unpublished).
18. Simmons, L. F. G., and Salter, C., "Experimental Investigation and Analysis of the Velocity Variations in Turbulent Flow," Proceedings of the Royal Society of London, Series A, Vol. 145, 1934.
19. Ducoffe, Arnold L., "A Report on the Design, Construction, Operation and Preliminary Calibrations on the Low Turbulence Wind Tunnel at the Georgia Institute of Technology," Navy Department, Office of Naval Research, Contract No. Nonr - 991 (01), May 1956.
20. Baines and Peterson, "An Investigation of Flow Through Screens," Transactions of the American Society of Mechanical Engineers, Vol. 73, July 1951.
21. Frenkiel, F. N., "The Decay of Isotropic Turbulence," Transactions ASME, Vol. 70, 1948, p. 311.
22. King, L. V., "On the Precision Measurement of Air Velocity by Means of the Linear Hot-Wire Anemometer," Philosophical Magazine, Series 6, Vol. 29, 1951, pp. 556-557.
23. Kennelly, A. E., Wright, C. A., and Van Bylevelt, J. S., Transactions of the American Institute of Electrical Engineers, Vol. 28, June 1909, p. 363.
24. King, L. V., "On the Convection of Heat from Small Cylinders in a Stream of Fluid: Determination of the Convection Constants of Small Platinum Wires with Applications to Hot-Wire Anemometry," Philosophical Transactions of the Royal Society of London, Vol. A 214, 1914, pp. 373-432.
25. Mock, W. C., Jr., and Dryden, H. L., "Improved Apparatus for the Measurement of Fluctuations of Air Speed in Turbulent Flow," NACA Technical Report No. 448, 1932.
26. Corrsin, S., and Uberio, M. S., "Spectrums and Diffusion in a Round Turbulent Jet," NACA Technical Note No. 2124, July 1950.

27. Lindvall, F. C., "A Glow Discharge Anemometer," Transactions AIEE, Vol. 53, 1943, p. 1068.
28. Werver, F. D., "An Investigation of the Possible Use of the Glow Discharge as a Means for Measuring Air Flow Characteristics," Review of Scientific Instruments, Vol. 21, 1950, p. 61.
29. Ling, S. C., Measurement of Flow Characteristics by the Hot-Film Technique, Ph.D. Dissertation, State University of Iowa, 1955.
30. Hubbard, P. G., Operating Manual for the II HR Hot-Wire and Hot-Film Anemometers, State University of Iowa, Studies in Engineering, Bulletin 37, 1957.
31. Ling, S. C., and Hubbard, P. G., "The Hot Film Anemometer: A New Device for Fluid Mechanic Research," Journal of Aeronautical Sciences, Vol. 23, 1956, p. 890.
32. Williams, F. J., "The Induction of Electromagnetic Forces in a Moving Liquid by a Magnetic Field, and its Applications to an Investigation of the Flow of Liquids," Proceedings of the Physical Society of London, Vol. 42, 1930, pp. 466-478.
33. Grossman, L. N., and Charwat, A. F., "The Measurement of Turbulent Velocity Fluctuations by the Method of Electromagnetic Induction," The Review of Scientific Instruments, Vol. 23, No. 12, 1952, pp. 741-748.
34. Grossman, L. M., and Shay, E. A., "Turbulent-Velocity Measurements," Mechanical Engineering, Vol. 71, 1949, p. 744.
35. Ippen, A. T., Tankin, R. S., and Raichlen, F., "Turbulence Measurements in Free Surface Flow with an Impact Tube-Pressure Transducer Combination," Massachusetts Institute of Technology, Hydrodynamics Laboratory, TR No. 20, 1955.
36. Ruetenik, J. R., "Development of a Miniature Pressure Transducer for Application to Airfoil Studies in the Shock Tube," WADC TR No. 58-629, 1958.
37. Perkins, F. E., and Eagleson, P. S., "The Development of a Total Head Tube for High Frequency Pressure Fluctuations in Water," MIT Hydro. Lab. TN No. 5, 1959.
38. Eagleson, P. S., Huval, C. J. and Perkins, F. E., "Turbulence in the Early Wake of a Fixed Flat Plate," MIT Hydro Lab. TR No. 46, February 1961.

39. Fage, A., and Townend, H. C. H., "The Distribution of Turbulence Over the Central Region of a Pipe," Technical Report of the Aeronautical Research Committee, Vol. 1, 1932033, p. 95.
40. Kovasznay, L. S. G., "Technique for the Optical Measurement of Turbulence in High Speed Flow, Heat Transfer and Fluid Mechanics Institute, Berkeley, Calif., 1949, p. 211.
41. Tsien, H. S., "On the Design of the Contraction Cone for a Wind Tunnel," Journal of Aeronautical Sciences, Vol. 10, No. 2, February 1943, pp. 68-70.
42. Smith, Richard H., and Wang, Chi-Teh, "Contracting Cones Giving Uniform Throat Speeds," Journal of Aeronautical Sciences, Vols. 11, 12, October 1944, p. 356.
43. Smoot, George F., and Yotsukura, Nobuhiro, Exploratory Tests of Turbulence Probe in Water Tunnel, United States Department of the Interior, Geological Survey, December 1962. (unpublished).